The Journal of Undergraduate Research in Physics

CONTENTS

VOLUME 4, NUMBER 1

SUMMER 1985

Published by Guilford College
for
The American Institute of Physics and The Society of Physics Students

THE JOURNAL OF UNDERGRADUATE RESEARCH IN PHYSICS

This journal is devoted to research work done by undergraduate students in physics and its related fields. It is to be a vehicle for the exchange of ideas and information by undergraduate students. Information for students wishing to submit manuscripts for possible inclusion in the Journal follows.

ELIGIBILITY

The author must have performed all work reported in the paper as an undergraduate. The subject matter of the paper is open to any area of pure or applied physics or physics related field.

SPONSORSHIP

Each paper must be sponsored by a full-time faculty member of the department in which the research was done. A letter from the sponsor to the editor must accompany the manuscript if it is to be considered for publication.

FORM

The manuscript should be typed, double spaced, on 8 1/2 x 11 inch sheets. Margins of about 1 1/2 inch should be left on the top, sides, and bottom of each page. Papers should be limited to twelve pages of text in addition to an abstract and appropriate drawings, pictures, and tables.

GENERAL STYLE

All papers must conform to the Style Manual of the American Institute of Physics. Each paper must be prefaced by an abstract that does not exceed 250 words.

ILLUSTRATIONS

Line drawings should be made with black India ink on plain white paper. If a graph is drawn on co-ordinate paper, the paper must be lined blue. Important lines should be ruled in black. Each figure or table must be on a separate sheet. Photographs must have a high gloss finish.

CAPTIONS

A brief caption should be provided for each illustration or table, but it should not be part of the figure. They should be listed together at the end of the manuscript.

EQUATIONS

Equations should appear on separate lines and may be written in black India ink.

FOOTNOTES

Footnotes should be typed double spaced and grouped together in sequence at the end of the manuscript.

SUBMISSION

Two copies of the manuscript and a letter from the sponsor should be sent to:
Dr. Rexford E. Adelberger, Editor
THE JOURNAL OF UNDERGRADUATE RESEARCH IN PHYSICS
Physics Department
Guilford College
Greensboro, NC 27410

SUBSCRIPTION INFORMATION

The Journal will be published biannually with issues appearing in Summer and Winter of each year. There will be two issues per volume.

TYPE OF SUBSCRIBER	PRICE PER VOLUME
Individual	$ 5.00
Institution	$10.00

Foreign subscribers add $2.00 for surface postage, $10.00 for air postage.

To receive a subscription, send your name, address, and check made out to The Journal of Undergraduate Research in Physics (JURP) to:

Journal of Undergraduate Research in Physics
Physics Department
Guilford College
Greensboro, NC 27410

BACK ISSUES

Back issues may be purchased by sending $10.00 per volume to the editorial office.

ISSN 0731 - 3764

The Journal of Undergraduate Research in Physics is published by Guilford College for the American Insititute of Physics and the Society of Physics Students.

VOLUME 4 1985

The Journal of Undergraduate Research in Physics

Published by Guilford College
for
The American Institute of Physics and The Society of Physics Students

ISSN 0731 - 3764

ON THE FOURTH YEAR OF PUBLICATION

An Editorial

As we start the fourth year of publication, I thought it of value to review the publication statistics of the first three volumes. A total of 136 pages of the Journal have been published in 6 issues as 24 separate articles. Five of the articles were authored by women. Eleven of the articles came from students at small colleges, institutions that only offer a bachelors degree, while the remaining 13 came from research institutions. There was the same split, 11 - 13, in articles coming from private and public institutions respectively.

The largest group of subscribers to the Journal continues to be members of the Society of Physics Students. A very important group of subscribers are the libraries. They not only archive the journal such that past volumes are available to students, but also provide the backbone of the financial support that is needed to publish. Over 160 libraries order copies for their journal collections. This, however, is only a small percentage of the schools that have a physics department in the United States. Subscribers who find that their campus library does not subscribe should get the administrative wheels rolling such that the Journal will be sent to their school.

Apparently there is a fair activity in undergraduate research outside the United States. Subscriptions are sent to over a dozen foreign countries. Two of the articles came from students outside of the United States. This trend is continuing as one can see by examining the table of contents of this issue. Two articles are from outside the US.

As with any enterprise such as this Journal, there is a lot of time invested by a number of people. Perhaps the least amount of work is in the publishing of the articles. The student authors, who do most of the work, receive the greatest benefit, not only from the recognition of publishing, but also learning to do real physics, rather than just studying about it. The group that I would like to recognize here are the faculty who sponsor the work done by the students. The time it takes for supervision and encouragement provided by these special faculty is seldom recognized as part of their teaching load. It is done because they feel that the only way to learn to do research is by doing it. Without faculty who are willing to do this, the physics research community would find that there are fewer and fewer students who will have the interest and committment to sustain it.

I am glad to see that the physics research groups such as the American Physical Society are beginning to recognize the importance of undergraduate research. Last year, Tak Leuk Kwok was awarded the Apker Award by the American Physical Society. This award was established to recognize the best piece of undergraduate research done in the US. I would like to point out that Mr. Kwok published an earlier piece of research in Volume 3, Number 1 of the Journal. It was good to get an independent verification that the quality of the research published in this Journal deserves national recognition.

CLASSICAL ELECTROMAGNETIC THEORY IN 3-d SPACE-TIME

C.C.H. Jui, J.V.A. Pari and J. Beauvais
Department of Physics
University of Ottawa
Ottawa, Ontario
Canada K1N 6N5

ABSTRACT

In this paper, we formulate electromagnetic theory in a hypothetical three dimensional space-time, assuming only Gauss' Law and the invariance of charge in this Minkowski space. The use of axial vectors and operators makes this formulation unique to three dimensions. We introduce two vector operators which serve as the two dimensional analogs of the cross product and curl. Using these operators, we obtain three equations involving a scalar magnetic field. These are analogous to three of the four Maxwell's equations of three dimensional space. These results are found to agree with the equations found from the four dimensional space-time STR-covariant tensor equations applied to three dimensional space-time. The magnetic field is found to satisfy the classical wave equation, but the electric field does not, even though it admits plane wave solutions.

INTRODUCTION

As physics is taught at the undergraduate level, it often appears that physical results are independent of dimensionality. For instance, the formalism of quantum mechanics is the same for any number of spatial dimensions. This is in general true only for physical theories involving polar operators within affine systems. However, when axial operators are used, such as in the case of electromagnetic theory, the results are not independent of dimensionality. As an example of this, we reformulate Maxwell's equations for a hypothetical universe which has only two spatial and one temporal dimension.

Vector Analysis

Vector quantities encountered in ordinary three space are of two kinds. Polar vectors, which include the force and velocity vectors, are distinguished by the property that upon mirror reflection, the components of these vectors in the mirror plane remain unchanged. Axial or pseudo-vectors, such as angular momentum, have projections that become inverted when subjected to a similar reflection. Strictly speaking, the latter are not vectors at all. They are, in fact, skew-symmetric second order tensors. A second order tensor can be represented as a square matrix.

Table 1 shows the number of free components in a skew-symmetric second order tensor as a function of the number of dimensions (dimensionality). For the special case of three dimensions (3-d), there are exactly

dimensionality	1	2	3	4	5	6	7
number of free components	0	1	3	6	10	15	21

Table 1
Number of free components versus dimensionality for a skew-symmetric second order tensor.

three independent components, allowing for a vectoral representation. In other dimensions, including the two dimensional (2-d) one, we lose the symmetry between the number of dimensions and the number of components.

This same distinction of types also applies to vector operators. This

means that axial operators, such as the curl (a monadic differential operator) and the cross product (a binary operator), defined in 3-d are unique to the 3-d geometry. Consequently, the 3-d electromagnetic theory, which makes extensive use of axial operators, cannot be transcribed directly into other dimensions.

For the purpose of this work, a reformulation of vector analysis is required to construct an electromagnetic theory applicable to 2-d. To this end, we introduce the "Greenian operator", which is expressed in a Cartesian coordinate system in 2-d space as:

$$G[x,y] \rightarrow [y,-x] \tag{1}$$

or in matrix form:

$$\underset{\sim}{G} = \begin{bmatrix} 0 & 1 \\ -1 & 0 \end{bmatrix} \tag{2}$$

Applying the Greenian operator to the 2-d 'del' operator, we obtain a new 'delta' operator:

$$\vec{\delta} = G\left[\vec{\nabla}\right] = \left[\frac{\partial}{\partial y}, -\frac{\partial}{\partial x}\right] \tag{3}$$

These will serve as the mathematical tools needed in our development of Maxwell's equations in 2-d (see section III).

Electromagnetic Theory in 2-d

I. Physical Postulates

We begin by assuming a linear universe with two spatial and one temporal dimensions (a Minkowski 3-space) with an affine coordinate system (x,y,t). We also will assume that electric charges are present in this universe, and that they are invariant under Lorentz transformations. We further postulate that Gauss' Law holds in this hypothetical world. This means that given any loop C enclosing a spatial region R, we have:

$$\oint \bar{E}\cdot\bar{n}\, dS = \frac{1}{2\epsilon_0}\iint \rho\, dA = \frac{Q}{\epsilon_0} \tag{4}$$

where $\bar{E}$ is the electromagnetic field, $\vec{n}$ the outward unit normal to C, ρ the charge density distribution and Q is the total charge enclosed by C.

II. Electrostatics

The assumption of Gauss' Law implies, for this universe, that a point charge q at the origin gives rise to a circularly symmetric electric field given by:

$$\bar{E}[\bar{r}] = \frac{q\,\bar{r}}{2\pi\epsilon_0 r^2} \tag{5}$$

Note that Coulomb's inverse square law is replaced by a 1/r field because of the two dimensional representation. The electrostatic potential for the point charge is:

$$\phi[r] = -\frac{q}{2\pi\epsilon_0}\ln[r] \tag{6}$$

assuming that $\phi(1) = 0$. Unlike the potential in 3-d, this potential function is not bounded, it does not approach an asymptotic limit at large distances.

In a similar manner, we can show that the electric field of an infinite line of charge with linear charge density λ has a uniform magnitude:

$$|\bar{E}| = \frac{\lambda}{2\epsilon_0} \tag{7}$$

and directed perpendicularly away from the line. Note the resemblance between this result and that for an infinite plane of charge in 3-d.

The differential form of Gauss' Law is:

$$\bar{\nabla}\cdot\bar{E} = \frac{\rho}{\epsilon_0} \tag{8}$$

Thus, the first of Maxwell's equations in 2-d is identical to the 3-d equation.

III. Moving Charges - Magnetostatics

Consider an infinite wire carrying equal charge densities λ of positive and negative charges moving in opposite directions at equal speeds v_0. The wire lies along the y = 0 line and a test charge q is moving at velocity v in the +x direction. From equation 8, the components of the electric field in

the rest frame S' of the test charge are given by:

$$E'_x = 0$$

$$E'_y = \pm \frac{\lambda'_+ - \lambda'_-}{2\epsilon_o} \begin{cases} + \text{ for } y>0 \\ - \text{ for } y<0 \end{cases} \quad (9)$$

where λ'_+ and λ'_- are the densities of the positive and negative carriers in the rest frame. One can derive the expression $(\lambda'_+ - \lambda'_-)$ by simple space-time relativity (STR), identical to the analogous case in 3-d given by Purcell (1):

$$\lambda'_+ - \lambda'_- = -2\lambda v v_o \gamma / c^2$$
$$\gamma = \left(1 - v^2/c^2\right)^{-\frac{1}{2}} \quad (10)$$

Substituting equation 10 into equation 9 gives:

$$\left|E'_y\right| = \frac{\lambda v v_o \gamma}{c^2 \epsilon_o} \quad (11)$$

Transforming back into the lab frame, the components of the force exerted on the moving test charge are:

$$\left|F_x\right| = 0 \quad (12)$$

$$\left|F_y\right| = q\lambda v v_o / c^2 \epsilon_o = qvI/c\epsilon_o$$

where $I = 2\lambda v_o$ is the electric current in the wire.

In general, it can be shown that a test charge moving in an arbitrary direction will experience a relativistic force perpendicular to its velocity, as in the 3-d case. However, the magnitude of the force in the 2-d case is independent of the position of the charge. For elegance of formulation, we shall write this relativistic force in terms of a "magnetic" field in analogy to the 3-d electromagnetic theory. In attempting to do this, we encounter some difficulties as a result of the reduction in spatial dimensionality. Recalling that in 3-d, the magnetic field is defined by the Lorentz force equation:

$$\overline{F} = q\left[\overline{E} + \overline{v}\times\overline{B}\right] \quad (13)$$

and is known to obey, in the static case, Ampere's Law:

$$\overline{\nabla}\times\overline{B} = \mu_o \overline{J} \quad (14)$$

As we try to find an equivalent representation in 2-d, we encounter the following problems when trying to transcribe equations 13 and 14:

(a) The cross product in not defined in 2-d.
(b) The curl is also not defined in 2-d.
(c) The magnetic field cannot be represented as a vector in 2-d.

The last difficulty arises because the 3-d magnetic field is an axial vector (it is defined in the Biot-Savart Law as a cross product of two polar vectors). An axial vector has 3 free components in 3-d representation, but only 1 in 2-d (see Table 1). Thus, the magnetic field must be a scalar field in 2-d representation. The difficulties in parts (a) and (b) can be resolved by using the new operators defined in the section on Vectors.

We define the magnetic field B in analogy to the 3-d field by the following force law:

$$\overline{F} = q\overline{E} + q\left[B\, G[\tilde{v}]\right] \quad (15)$$

For the case of an infinite wire at y = 0 carrying a current I in the +x direction, we have:

$$B = \pm \frac{\mu_o}{2} I \quad (16)$$

where the + and - signs correspond to the regions $y>0$ and $y<0$. For this simple case, the difference in the values of B at the endpoints of any directed path from point P to point Q is proportional to the total current through the path:

$$\left|B(Q) - B(P)\right| = \mu_o I \quad (17)$$

This relationship between field and current can be generalized for any current density distribution J to give

the 2-d analog of Ampere's Law:

$$B(Q) - B(P) = \mu_o \int_\Gamma -\bar{J} \cdot G(\bar{dS}) \quad (18)$$

where Γ is any directed path from P to Q with line element $\bar{ds}$. Applying equation 18 to directed line segments parallel to the x and y axes, and taking the limit that Q approaches P, for a static current distribution we have:

$$\bar{\delta} B = \mu_o \bar{J} \quad (19)$$

This is analogous to equation 13 for 3-d. Using this equation, we may develop a 2-d Biot-Savart Law, using a vector potential as an intermediate step.

IV. Induction and Displacement Current

We define the magnetic flux ϕ_m in the region R as follows:

$$\phi_m = \iint_R B \, dA \quad (20)$$

This definition of the magnetic flux results in an induced voltage (e.m.f.) in the current loop enclosing R given by the same relation (Faraday's Law) as in 3-d:

$$\epsilon = - \frac{\partial \phi_m}{\partial t} \quad (21)$$

The details of the derivation are given in Purcell (1) and apply to both the 3-d and 2-d configurations.

The e.m.f. is defined in 2-d in the same manner as in 3-d:

$$\epsilon = \oint_\Gamma \bar{E} \cdot \bar{dS} \quad (22)$$

Using our new 'delta' operator (Equation 3), Green's theorem can be re-written as:

$$\oint_\Gamma \bar{E} \cdot \bar{dS} = - \iint_R (\bar{\delta} \cdot \bar{E}) \, dA \quad (23)$$

When this is substituted into Faraday's Law in 2-d (equation 21) we obtain:

$$\iint (\bar{\delta} \cdot \bar{E}) dA = \frac{\partial \phi_m}{\partial t} = \iint \frac{\partial B}{\partial t} \, dA \quad (24)$$

Equating the two integrands yields:

$$\bar{\delta} \cdot \bar{E} = \frac{\partial B}{\partial t} \quad (25)$$

This is analogous to the third of Maxwell's equations in 3-d:

$$\bar{\nabla} \times \bar{E} = - \frac{\partial \bar{B}}{\partial t} \quad (26)$$

As in the 3-d formulation, the concept of a displacement current is required. The derivation is, in fact, independent of dimensionality, as only polar vectors and operators are involved. (2) We write the displacement current density as:

$$\bar{J}_D = \epsilon_o \frac{\partial \bar{E}}{\partial t} \quad (27)$$

This is identical to the definition in 3-d. Adding this term to the free current, equation 20 becomes:

$$\bar{\delta} B = \mu_o \left[\bar{J} + \bar{J}_D \right] \quad (28)$$

Substituting equation 27 into equation 28 gives:

$$\bar{\delta} B - \mu_o \epsilon_o \frac{\partial \bar{E}}{\partial t} = \mu_o \bar{J} \quad (29)$$

which is the analog of the fourth of Maxwell's equations in 3-d:

$$\bar{\nabla} \times \bar{B} = \mu_o \bar{J} + \mu_o \epsilon_o \frac{\partial \bar{E}}{\partial t} \quad (30)$$

Equations 8, 25, and 29 are the analogs of three of the four Maxwell's equations in 3-d. The only equation without an analog is:

$$\bar{\nabla} \cdot \bar{B} = 0 \quad (31)$$

Since B is a scalar field in 2-d, it appears that no analog exists for

equation 31. This will be confirmed in the next section, where a STR-covariant formulation in 2-d, using the same formalism as in 3-d, will show that there are only 3 Maxwell's equations in 2-d. In this way, the apparent symmetry in the electric and magnetic fields seen in the free-space Maxwell's equations is not preserved in the transition from 3-d to 2-d.

V. STR-Covariant Formulation

An alternate formulation of electromagnetic theory in 3-d is possible by exploiting the 4-vector formulation of STR. This derivation is discussed in detail elsewhere (3). For our hypothetical world (a Minkowski 3-space), we may use a similar 3-vector formulation using the following affine coordinate system:

$$x_1 = x;\ x_2 = y;\ x_3 = ict \tag{32}$$

in which the density 3-vector is written as:

$$J_\alpha = \{ J_x,\ J_y,\ ic\rho \} \tag{33}$$

and the electromagnetic field tensor E, a skew-symmetric 2nd order tensor, is written as the matrix:

$$E_{\alpha\beta} = \begin{bmatrix} 0 & B & -iE_x/c \\ -B & 0 & -iE_y/c \\ -iE_x/c & -iE_y/c & 0 \end{bmatrix} \tag{34}$$

We then apply the state equations (just the same as those for 4-d space-time):

$$(\delta E)_{\alpha\beta\gamma} = \frac{\partial E_{\alpha\beta}}{\partial x_\gamma} + \frac{\partial E_{\beta\gamma}}{\partial x_\beta} + \frac{\partial E_{\gamma\alpha}}{\partial x_\alpha} \equiv 0 \tag{35}$$

$$E_{\alpha\beta\beta} = \sum_\beta \frac{\partial E_{\alpha\beta}}{\partial x_\beta} = \mu_0 J_\alpha \tag{36}$$

In this case, the Greek indices can take on the values 1,2,3. Equation 35 is symmetric in the indices (cyclic permutations do not alter the equation). This property, in addition to the skew-symmetry of the field tensor, reduces equation 35 to a single scalar equation:

$$\frac{\partial E_x}{\partial y} - \frac{\partial E_y}{\partial x} = \frac{\partial B}{\partial t} \tag{37}$$

which is identical to equation 25.

Solving equation 36, we get three scalar equations:

$$\alpha = 1 \quad \frac{\partial B}{\partial y} - \frac{1}{c^2}\frac{\partial E_x}{\partial t} = \mu_0 J_x \tag{38}$$

$$\alpha = 2 \quad \frac{\partial B}{\partial x} - \frac{1}{c^2}\frac{\partial E_y}{\partial t} = \mu_0 J_y \tag{39}$$

$$\alpha = 3 \quad \frac{\partial E}{\partial x} + \frac{\partial E}{\partial y} = \frac{\rho}{\epsilon_0} \tag{40}$$

Equations 38 and 39 reiterate the vector equation 29 and equation 40 restates the divergence law of equation 8.

Thus, the tensor form of the Maxwell's equations is invariant with respect to dimensionality. However, the physical consequences as seen through vector analysis appear to be very different in 2-d as compared to 3-d.

VI. Radiation

We now shall attempt to derive wave equations for the E and B fields in a vacuum. In free space, our Maxwell's equations are:

$$\bar{\nabla} \cdot \bar{E} = 0 \tag{41}$$

$$\bar{\delta} \cdot \bar{E} = \frac{\partial B}{\partial t} \tag{42}$$

$$\bar{\delta} B = \epsilon_0 \mu_0 \frac{\partial \bar{E}}{\partial t} \tag{43}$$

Applying the operator to equation 43 gives:

$$\bar{\delta} \cdot (\bar{\delta} B) = \delta^2 B = \mu_0 \epsilon_0 \frac{\partial}{\partial t}(\bar{\delta} \cdot \bar{E}) \tag{44}$$

Substituting equation 42 into equation 44, we get:

$$\delta^2 B = \frac{1}{c^2}\frac{\partial^2 B}{\partial t^2} \tag{45}$$

where $\delta^2 = \left[\frac{\partial}{\partial y}, -\frac{\partial}{\partial x}\right] \cdot \left[\frac{\partial}{\partial y}, -\frac{\partial}{\partial x}\right] = \nabla^2$

Hence we get the relationship:

$$\nabla^2 B = \frac{1}{c^2}\frac{\partial^2 B}{\partial t^2} \qquad (46)$$

which shows that the magnetic field satisfies a homogenous ideal wave equation in free space.

Doing the same for the electric field yields:

$$\bar{\delta}\left[\bar{\delta}\cdot\bar{E}\right] = \left[\frac{\partial^2 E_x}{\partial y^2} - \frac{\partial^2 E_y}{\partial x\,\partial y}, \frac{\partial^2 E_y}{\partial x^2} - \frac{\partial^2 E_x}{\partial x\,\partial y}\right] \qquad (47)$$

$$= \frac{1}{c^2}\frac{\partial^2 \bar{E}}{\partial t^2}$$

which is not in the form of the ideal wave equation. The form of the wave equation is invariant under orthogonal transformations of space-time coordinates (Lorentz transformations). (4) Thus, the electric field does not satisfy a classical wave equation. Never-the-less, equation 47 does admit plane-wave solutions, for instance:

$$\bar{E}(x,y,t) = \hat{y}\, E_0 \cos(kx - \omega t) \qquad (48)$$

where $\omega / k = c$, with the electric field oscillating perpendicular to the direction of propagation. There is no freedom in the mode of polarization, as there is only one transverse degree of freedom.

CONCLUSIONS

We have shown that in 2-d space, there are only three Maxwell's equations. It is seen that our vectoral derivation from simple postulates gives the same results as the general tensor formulation. The most surprising aspect of our results is that the electric field does not satisfy the classical wave equation. It appears that the presence of harmonic electromagnetic radiation in the physical world is primarily the result of the dimensionality of our universe. In fact, the 2-d circular symmetrical solution of the wave equation has a radial part which is oscillating, but not periodic. Thus, it seems that a 3-d universe is unique in possessing many properties which we take for granted.

ACKNOWLEDGMENTS

We would like to thank Mandhir Dhesi and Michael Cashion of the University of Ottawa for their assistance in proof reading the manuscript and in the manual layout of the equations.

REFERENCES

(1) E.M. Purcell, Electricity and Magnetism, (Berkeley Physics Course, Vol. 2), McGraw-Hill, New York, 1965

(2) See Chapters 11 and 12 of Purcell (1) for the discussion in 3-d.

(3) D.F. Lawden, An Introduction to Tensor Calculus and Relativity, Chapman and Hall, London, 1975.

(4) W.T. Rossman, Department of Mathematics, University of Ottawa, private communication.

FACULTY SPONSOR OF THIS PAPER

Dr. A Manoogian
Department of Physics
University of Ottawa
Ottawa, Ontario
K1N 6N5 Canada

WIND AND SOLAR ENERGY IN NORTHEAST IOWA *

Samuel P. Benz and Stephen D. Nelson
Physics Department
Luther College
Decorah, IA 52101

ABSTRACT

Wind and solar energy in Northeast Iowa were studied during 1984-85. By comparing wind energy at two sites, it is shown that location has a strong influence on wind energy. Wind power is shown to be different from wind speed. Weekly averages of wind and sun energy are found to be complementary on a seasonal basis.

INTRODUCTION

This research project is a study of wind power and solar power and their suitability as energy sources in northeastern Iowa. This type of experiment has already been does at Iowa State University (1) and at Luther College (2). It is the intent of this experiment to compare the collected data with previous long term results and to see how location affects the wind power.

By incorporating our results with those of Takle and Shaw (1), we hope to show that the conclusions made at Iowa State University also hold true in Northeast Iowa. Our data, collected between May 1984 and January 1985, measured the deviations in wind power at two different sites. This limited data set, when viewed in the context of existing data, allowed us to determine the effectiveness of a favorable location.

THEORY

The power available from the wind is proportional to the cube of the wind speed. The meteorological wind power per area is given by:

$$\frac{P}{A} = \frac{v^3 \rho}{2} \qquad (1)$$

where P/A is the power per area (watts/m^2), v the wind speed, and ρ the average density of the air (1.29 kg/m^3).

It should be noted that the average wind speed does not give the correct value for the average wind power. When the wind speed varies, the higher wind speeds give a much larger contribution to the average wind power than the lower speeds. To study this effect, we picked two sites with different wind speed profiles.

Luther College is set in a large river valley, surrounded by many small hills and bluffs. Site 1 is located on the Luther College Campus. The anemometer is located on the top of the science building. There are many trees and buildings nearby to disturb the air flow. These obstructions, as well as the geographic location, make this site unfavorable.

Site 2 is located at the Luther College Observatory, eight miles north of Site 1. This site lies on a flat plain, surrounded by fields. The anemometer is ten meters from the ground on the top of a pole. It is effectively the highest point in relation to the surrounding area, with no obstructing buildings or trees. This site is indicative of possible sites for a wind generator for the northeast Iowa region.

DATA ACQUISITION

At each site we have a Commodore VIC-20 dedicated to monitoring the wind energy. At Site 2, a non-interruptable battery backup was used to alleviate

power outage problems. The computer at Site 1 also monitors the solar energy for the area. The anemometers are of the "contact type", obtained from M.C. Stewart, Ashburnham, MA 01430. A four-cup wheel on a vertical spindle is geared to close a reed switch once for the passage of each 1/60 th mile of wind. This switch is connected to the CB1 input of the VIC-20 user port. The wind speed is found by determining the time between closings of the switch, using the internal clock of the computer. This method, when compared with a calibrated anemometer, gave a close approximation to the instantaneous wind speed.

We found the average wind speed cubed over a 7.5 minute interval using the following formula:

$$\langle v^3 \rangle = \frac{1}{T} \sum_i v_i^3 \, \Delta t_i \qquad (2)$$

where v is the instantaneous wind speed and t is the time interval between closings, and T is the total elapsed time (7.5 minutes). The values for the the average of the cube of the wind speed were stored in the computer memory, averaged at the end of the day, and then stored on a tape deck. The average wind speed for each day was also collected. This information is interesting in itself, but is is also a good check to see if the collected values of the wind power are reasonable. The wind speed data was found in the same manner as equation 2:

$$\langle v \rangle = \frac{1}{T} \sum_i v_i \, \Delta t_i . \qquad (3)$$

To determine the energy from the sun, an Epply Precision Spectral Pyranometer Model P5P was used as the transducer. The device is on the roof of the science building at Site 1, with nothing obstructing the sunlight. The output of the pyranometer is amplified and sent to an 8-bit analog-to-digital converter. The computer samples the ADC output eight times each hour. These values are adjusted such that the stored values are the solar insolation in Joules/m^2. This solar data acquisition system has been in operation since 1976.

RESULTS

To analyze the data, we reduced wind speed cubed and solar energy values to weekly and monthly averages. Since we are interested in making realistic comparisons in solar and wind generated electricity, we multiplied the raw wind energy available by a factor of .3 which is typical or the efficiency of an average wind driven electrical generator (3). No reduction was done

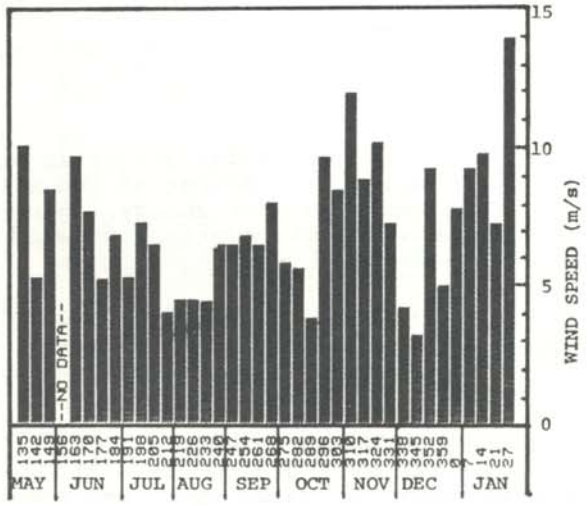

FIGURE 1
Weekly averaged wind speed at Site 2 by the end of the week day number and month.

for the solar energy (insolation); 10% efficiency could be used if a panel of photovoltaic cells were used to produce electricity; while a 50% efficiency could be used if thermal energy were accumulated. The wind velocity data was converted to power/area using equation 1 and then to KWH/m^2, the standard commercial electrical energy unit for comparing collected energy sources. The solar energy is converted using the formula:

$$10^6 \, J/m^2 = 0.2778 \, kWh/m^2 \qquad (4)$$

Figure 1 shows the average wind speed measured. The effect of the varying wind speed on the wind power can be seen in Figure 2. There are very large changes in the wind power and relatively small changes in the wind velocity profile. This is due to the fact that the wind power is proportional to the instantaneous wind speed cubed and not the cube of the average wind speed.

Examination of Figures 2 and 3 shows the difference in the wind energy

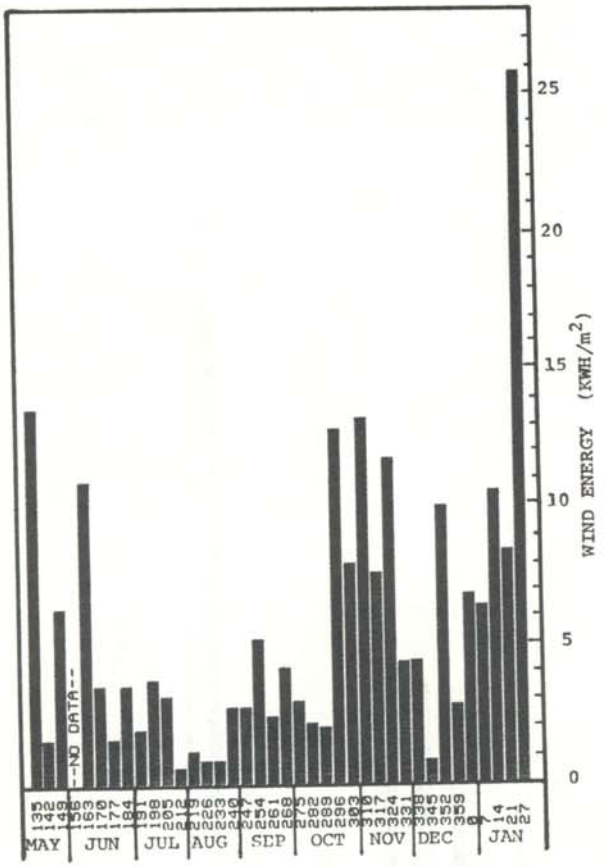

FIGURE 2
Weekly averaged wind power at Site 2 by end of week day number and month.

collected at the two sites. Clearly location makes a substantial difference in t he amount of wind energy collected. Our results indicate that at Site 2, with its open, uninhibited surroundings and higher relative elevation, here was appoximately four times more energy available than at Site 1. Thus, location is an important factor when considering the performance of a wind-powered generator. Because of this, Site 2 will be used in further comparisons of results.

We will compare our results with the previous observations of Takle and Shaw (1). Using Fourier analysis of

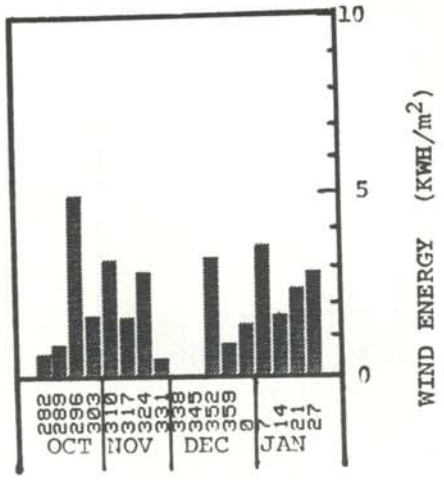

FIGURE 3
Weekly averaged wind power at Site 1 by end of week day number and month.

logarithmically averaged data over an entire year span, they derived results for the expected average meteorological solar and wind power per area (see Figure 4). Although our data has been corrected for practical use, it should be noted that our location (Site 2) has

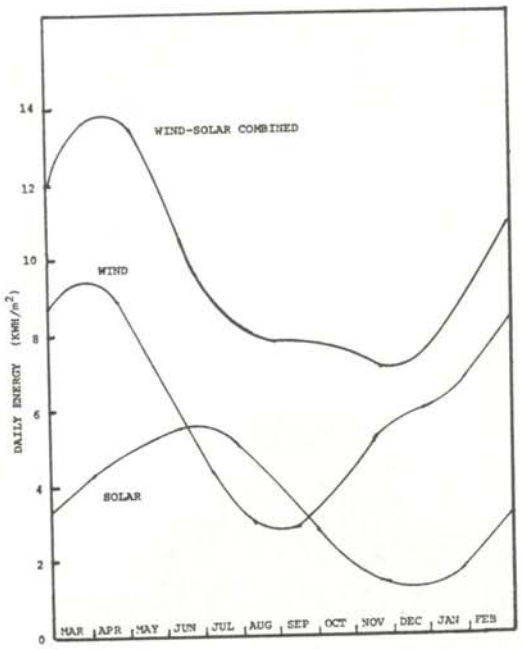

FIGURE 4
Predicted meteorological daily energies for wind, solar and wind-solar combined (1).

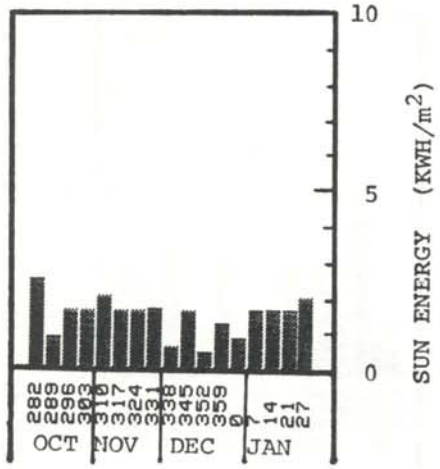

FIGURE 5
Weekly averaged solar power by end of week day number and month.

more wind energy available than the average. The general slope of our curve does seem to follow the expected results with the minimum occuring in June, July, and August and higher relative values in November, December, and January. Our data fluctuates more than that of Takle and Shaw because we have used weekly averages.

The solar data, which was collected during October through January, seems to be fairly consistent at about 2 KWH/m² (see Figure 5). This data also agrees with the curve of Takle and Shaw. Their minimum in December is more noticeable than ours because of its time averaged nature, whereas we have data only spanning one winter. To make a more meaningful comparison of the solar energy in northeast Iowa to the results of Takle and Shaw, the results of the 1977 study (2) are examined (see Figure 6). Note the maximum occuring during the summer months.

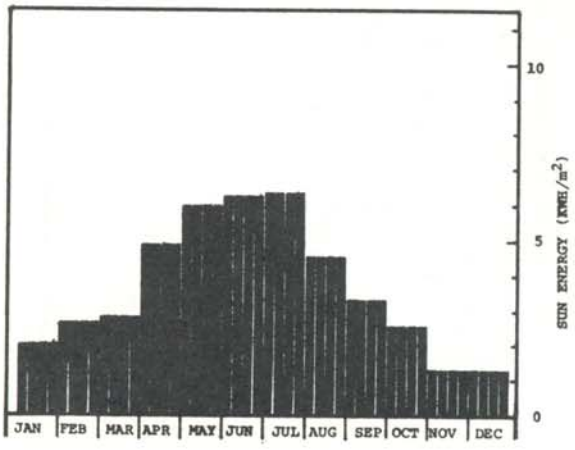

FIGURE 6
Monthly averaged solar power for 1977 (2).

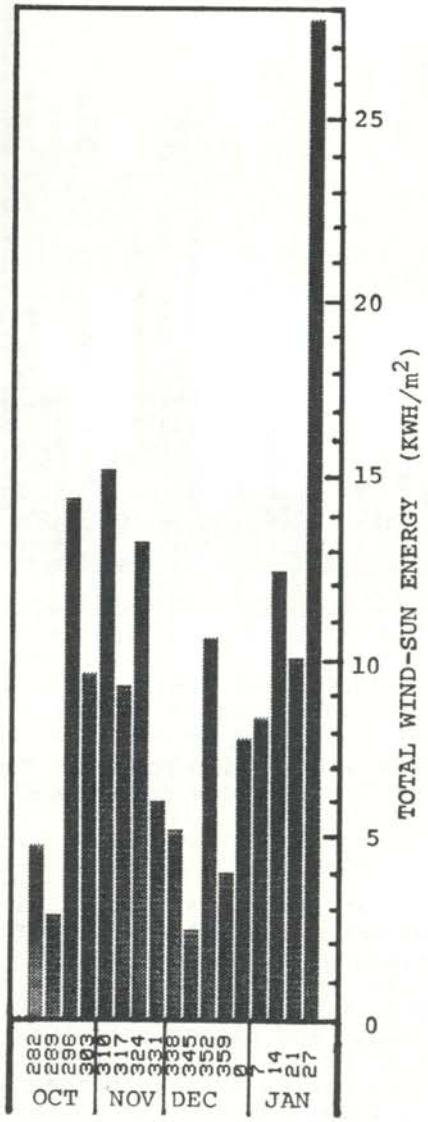

FIGURE 7
Combined weekly averaged solar and wind power by end of week day number and month. This is the sum of the results shown on Figures 2 and 5.

When we combine wind and solar energy together, we find that the seasonal minima and maxima are complementary (see Figures 4 and 6). This is noticeable in the data of Tackle and Shaw, where the total energy curve fluctuates less than the sun and wind energies separately. Our data (Figure 7) shows the same trend. Thus, if a station uses both wind and solar collectors, it provides a much more consistent and flexible energy system.

ACKNOWLEDGMENTS

The authors would like to thank Paul Hink for his help in getting this project started. We would also like to thank Rod Tressel for keeping the project going during the summer months, and Eric Bierstadt for his computer assistance. We would like to thank Ken Larson, Tim Lecander, Seth Vongsaga and Brad Baalson for their help. Finally, we would like to thank Dr. Dennis Barnaal for his advice and supervision.

REFERENCES

* This research was sponsored by the Society of Physics Students under a 1984 Bendix Award.

(1) E.S. Takle and Shaw, R.H., "Combined Renewable Energy Resources (Solar and Wind) for Iowa", Report to the Iowa Energy Policy Council, December 1977.

(2) D.E. Barnaal, "Wind and Insolation Studies in Northeast Iowa for 1976 and 1977", Report to the Iowa Energy Policy Council, June 1978.

(3) E.S. Takle and Brown, J.M., "Wind and Wind Energy in Iowa", Report to the Iowa Energy Policy Council, October, 1976.

FACULTY SPONSOR OF THIS PAPER

Dr. Dennis Barnaal
Physics Department
Luther College
Decorah, IA 52101

PERCOLATION THRESHOLD IN UNUSUAL LATTICES

Martin Schulte and Peter Sprenger
Institutue of Theoretical Physics
Cologne University
5000 Koln 41
Federal Republic of Germany

ABSTRACT

We determined the threshold probability p_c for percolation in a pentagon lattice where each unit cell has five corners. The calculations, written in Fortran V, use the Hoshen-Kopelman algorithm. Our results are consistent with predictions of Waldor et. al. (1).

(1) H.M. Waldor, W.F. Wolff, and J. Zittartz, Phys. Lett. A, 104, 355.

INTRODUCTION

Imagine a fisherman's net. This net consists of many strings and knots. The knots hold the strings together. After a few years of extensive use, the net becomes worn and many strings and knots are missing. When we count the remaining strings and knots, we find that they are set randomly in the original shape of the net, with some probability p. As more knots and strings disappear, the probability p of finding an unbroken knot or string decreases, and at some point $p = p_c$, the net separates into two parts. Our problem is to determine this threshold probability p_c for a particular shaped net. Since there is more than one string attached to a knot, one has to be concerned whether a knot breaks or a string breaks.

This story can be transformed into more scientific language: the strings become bonds; the knots become sites and the net a cluster. The probability at which the net splits into two parts is the percolation threshold.

PROCEDURE

We separate our task into two parts: finding the bond percolation threshold and the site percolation threshold for different lattice types. The values for the threshold probabilities for square and honeycomb lattices have been calculated by others and are well known. This paper reports our calculations to determine these values for the pentagon lattice, where each unit cell has five corners (1). Our programs to calculate the percolation thresholds, written in FORTRAN V, use the Hoshen-Kopelman algorithm and the well known method of determining p_c by iteration for one lattice size (2). We do the calculations for a number of different finite lattice sizes and then extrapolate to find the percolation threshold for an infinite lattice.

RESULTS

Using the methods described above, we get the following results when extrapolating to infinite lattices:

- p_c bond percolation for a pentagon lattice: (0.579 ± 0.001) (See Figure 1).
- p_c site percolation for a pentagon lattice: (0.628 ± 0.001) (See Table 1)
- p_c site percolation for a four-dimensional lattice: (0.196 ± 0.002) (See Table 1)
- p_c bond percolation for a four-dimensional lattice: ($0.160 \pm .0005$) (3).

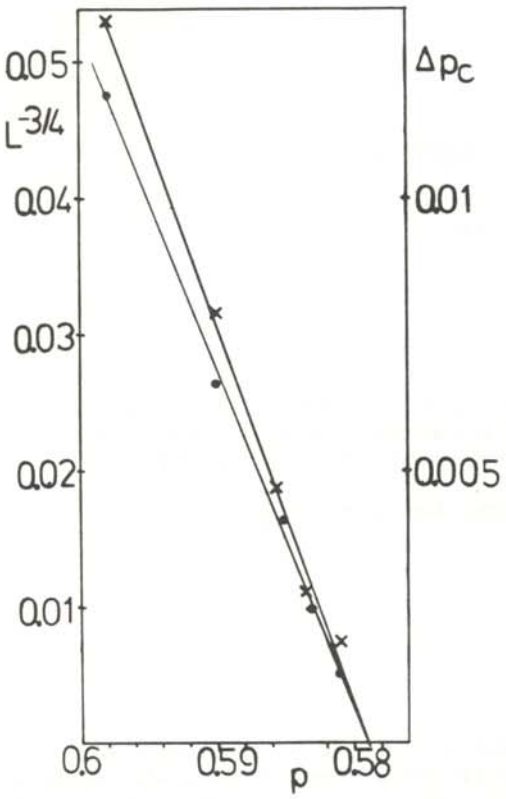

FIGURE 1
A plot of $L^{3/4}$ (left scale crosses) and Δp_c (right scale dots) versus concentration p for pentagon lattice site percolation. The data are expected to asymptotically approach straight lines ending at the same percolation threshold p_c as indicated in this figure.

The critical exponent ν (where the standard deviation for the percolation threshold $\Delta p_c \propto L^{-1/\nu}$) was found to be consistent with $\nu = 4/3$. This is the accepted two-dimensional value (2) for both bond and site percolation.

CONCLUSIONS

Table II shows that the p values for the pentagon lattice interpolates the values of the square and honeycomb lattice. We also show that Waldor et al's prediction (1) that p_c is close to .574 is good. The value for matches the results known for other lattices. For the four-dimensional lattice, we improved the known values for site percolation and confirmed the more accurate series result (4) for bond percolation.

Site percolation in the pentagon lattice

L	N	p_c	Δp_c
400	75	.627479	.003726
300	150	.627388	.004673
200	125	.626452	.006337
100	537	.625212	.010484
50	375	.622840	.016785

Site percolation in the four-dimensional lattice

30	60	.197965	.003175
25	60	.199268	.003600
20	50	.199922	.005220
17	50	.200840	.006217
13	50	.202598	.009107
10	60	.205013	.013913

TABLE I
Computer generated data for site percolation for the pentagon and four-dimensional lattice. L is the system size and N the number of runs.

REFERENCES

(1) M.H. Waldor, W.F. Wolff, J. Zittartz, Phys. Lett. A, 104, 355.

(2) D. Stauffer, Introduction to Percolation Theory, Taylor and Francis, London, 1985.

(3) D. Stauffer, private communication.

(4) J. Adler, A. Aharony, A.B. Harris, Phys. Rev. B, 30, 2832, (1984); D.S.Gaunt, M.F. Sykes, H. Ruskin, J. Phys. A9, 1899, (1976).

FACULTY SPONSORS OF THIS PAPER

A. Weinkauf and D. Stauffer
Institute of Theoretical Physics
Cologne University
5000 Koln 41
Federal Republic of Germany

	bond	site
triangular	0.347	0.5
square	0.5	0.593
pentagon	0.579	0.628
honeycomb	0.653	0.696

TABLE II
Results for bond and site percolation thresholds for various lattice shapes.

QCD, LATTICE GAUGE THEORY, MONTE CARLO CALCULATIONS AND INSTANTONS

Rodney Kinney
Physics Department
Caltech
Pasadena, CA 91125

ABSTRACT

A method is introduced to better study quantities which are related to the topological charge in lattice guage theory of Quantum Chromodynamics. The method will use global Monte Carlo steps to calculate the relative weights of the topological sectors, while separate runs are performed in each sector. The Monte Carlo procedure is modified to prevent tunneling between sectors by restricting the action density to be less than 0.25 per plaquette. This value will, we hope, be small enough to prevent tunneling yet large enough not to affect the dynamics of the lattice.

INTRODUCTION

Quantum Chromodynamics (QCD) is a theory that was introduced about a decade ago in the hope of providing a complete explanation of the observed behavior of the strong force. So far, QCD has provided impressive predictions that indicate that it could be the theory for which physicists are looking, and has collected a large following. A thorough review of QCD can be found elsewhere (1).

QCD is a quantum field theory in which quarks and gluons interact amongst themselves . The theory is a Lagrangian field theory. One defines a Lagrangian density L. The expectation of any physical observable is given by:

$$\langle O \rangle = \frac{1}{Z} \int O[L'] \; e^{-iS} \; dL'$$

$$S = \int L' \; d^3x \; dt \qquad (1)$$

$$Z = \int e^{iS} \; dL'$$

where S is tha action of the Lagrangain density L', O(L') is the value that the observable taken for the particular field configuration L' and Z is a normalization factor. The integrations dL' are over all possible forms of the Lagrangian field, a difficult operation to carry out or even to define. The imaginary exponent introduces oscillations which are difficult to manage. Matters can be simplified by the variable change:

$$t \rightarrow t' = -it \qquad (2)$$

This makes the time dimension equivalent to the three spatial dimensions. Physical results may be retrieved by analytically continuing back into real time. The rest of this paper will deal with Euclidean four dimensional space: three spatial dimensions and one imaginary temporal dimension.

Pseudo-particles

The main contributing terms to the integrand of Equation 1 over configurations are those for which the action is minimal. Finding these configurations amounts to solving the set of field equations which are derived from the classical Euler-Lagrange equations used for solving Hamilton's principle of least action (2). The solutions which minimize the action are called topological solitons (also pseudo-particles), and have been the

subject of much study, both as they relate to QCD (as well as solid state and plasma physics) and as purely mathematical objects.

In four-dimensional Euclidean space, there is a pseudo-particle called the instanton. One can define a quantity, called the topological charge q, which takes on only integral values and depends on the configuration of the Lagrangian field. Configurations can be divided into groups with different q, said to belong to different topological sectors. One can prove that continuous infintesimal changes to a configuration cannot bring it into a different topological sector. Thus, topological charge is conserved. The q=0 solution is trivial: the vacuum. When the solution for the q=1 case was found (3), it was called the instanton. The physical interpretation of pseudo-particles is not certain, but their existence has been used to solve some symmetry-breaking problems that have plagued QCD in the past (4).

Lattice Gauge Theories

One parameter that emerges in QCD is the coupling constant g. While the mathematics of QCD are too complicated to solve exactly, results often can be obtained through perturbation theory, usually expanding about small g. Recently, a new approach to QCD has been taken in order to study the region out of the realm of perturbation theory, that of strong coupling. The method consists of defining the theory on a lattice, a four-dimensional hypercubical lattice of points separated by links of finite length. Associated with each link is a matrix of a particular group. For our studies, we have used the group SU(2). The field is defined on the links of the lattice such that when a particle moves from one site to another, its (vector) wave function becomes multiplied by the matrix of the link between the two sites. In a properly defined limit of lattice spacing (going to zero), the continuum theory is retrieved, and physical results can be obtained. A complete review of lattice gauge theories can be found elsewhere (5).

The action in a lattice gauge theory is defined as follows. Consider four sites at the corners of a square of the smallest size that the lattice spacing will allow. Such a square is called a plaquette. The transporter, U, around the plaquette is the matrix that is the product of the matrices associated with the links that are the sides of the plaquette. The action of the entire lattice is obtained by summing over all plaquettes:

$$S_t = B \sum_i S_i \qquad B = 4/g^2$$

$$S_i = 1 - 1/2 \ \mathrm{Re}\left[\mathrm{Tr}\{U_i\}\right] \tag{3}$$

where S_i is the action of the ith plaquette.

The expectation value of physical observables is defined in the same manner as in the continuum case, except that for lattice theories, the integral over all possible configurations becomes a sum that one can define and even evaluate. To obtain all possible configurations of the field, one merely has to vary the matrices of the links throughout all combinations of values. Of course, this is still not a very practical thing to do. Instead, one examines the expression for the averages of the observables:

$$\langle O \rangle = 1/Z \ \Sigma O \ e^{-BS}$$

$$S = \sum_i S_i \tag{4}$$

The first sum is over all possible values of the link matrices. The second sum is over all the plaquettes.

One can see that with the correspondences:

$$B \longrightarrow 1/kT \tag{5}$$

and

$$S \longrightarrow \text{Energy} \tag{6}$$

one has the same expressions that appear for observables in a statistical system at temperature T. The problem of QCD with large coupling constant becomes analogous to a four-dimensional statistical system at high temperature. Weak coupling corresponds to a system at low temperature. At this point, one can turn to methods used by statistical physicists using computers to simulate systems in thermal equilibrium. The method most often used is that of Monte Carlo.

Monte Carlo Simulations

Monte Carlo simulations in lattice QCD start with the system in some initial configuration. From there, small changes in the system are offered. New configurations are accepted with a Boltzmann probability:

$$e^{-B[S_{new} - S_{old}]} \qquad (7)$$

(If $S_{new} < S_{old}$, the probability of acceptance is 1.) Eventually the system reaches thermal equilibrium and the measurable quantities can be determined directly.

Simulations on the lattice run into problems when confronted with matters that have to do with topological charge. First of all, topological charge is difficult to define on the lattice. Some definitions have been presented (6), but they are complicated and take much time for a computer to work out. They also do not always give the correct value for the observable. Another major problem is that any configuration on the lattice can be deformed into any other by continuous changes of the links. Topological charge therefore is not conserved. In measuring values of the quantities such as $\langle q^2 \rangle$, the system is constantly tunneling between topological sectors. One must continually calculate q in order to be sure in which sector one is presently. The work we are carrying out is an attempt to resolve these problems and allow Monte Carlo studies of different topological sectors on the lattice.

CALCULATIONS

The idea is to perform separate runs in each topological sector. We modify the Monte Carlo procedure so that the system cannot tunnel. We then perform runs starting from a configuration of whose charge we are certain, and never have to compute the charge again. The value of any observable will be the average of its value in all of the sectors, with appropriate weighting. The relative weights of the sectors can be found in a straight forward manner. The ratio of the weights of two sectors is the ratio of the probabilities for each to go into the other as given by the Boltzmann probability.

Preventing tunneling

The topological charge cannot change gradually. It must change from one integer to another, and that change must take place at one particular step, at one particular link. If one can isolate the step which causes the tunneling, one can prevent the change. It has been shown (7) that there is a minimum energy density in the vicinity of the link that changes the charge. This means that at least one plaquette will have an action greater than a certain value, which is called epsilon. This epsilon is independent of both lattice size and the coupling constant (B). If the Monte Carlo updating procedure simply does not accept any configuration which has plaquettes of action greater than epsilon, then the system cannot tunnel. The problem has been to find an epsilon which is large enough not to interfere too severely with the behavior of the lattice, but which will still prevent tunneling.

Monte Carlo runs were made on an SU(2) lattice of seven sites in each direction (a typical size). Candidate configurations were generated by going link by link through the lattice. Each link was multiplied by a random matrix close to the identity matrix. Once that change had been accepted or rejected, we moved on to the next link, and so on. The process of going once through the lattice and updating each link is called one sweep.

An instanton on the lattice, left to itself at zero temperature (infinite B), normally will decay into the vacuum in about 200 sweeps. We tested our epsilon condition by performing runs at infinite B with different epsilons and watching for the instanton to decay into the vacuum. Those that did not decay, froze into a state in which any change would either increase the action (and thus be rejected by the Boltzmann condition at zero temperature) or violate the epsilon condition. The system remained stationary in the q=1 sector.

Table 1 shows a run with epsilon equal to .245. The frames show plaquette energies in a single plane of the hypercube. This set of values shows an instanton that has been subjected to several sweeps at a very high temperature. The boiling has obliterated any trace of the instanton. If the epsilon condition restraint is

.000	.021	.077	.066	.022	.051
.118	.017	.010	.028	.244	.006
.022	.013	.020	.002	.002	.009
.015	.000	.013	.011	.048	.013
.025	.031	.004	.035	.002	.001
.027	.024	.003	.014	.003	.012

TABLE 1
Plaquette energies in a single plane of the hypercube. The distribution of energies is characteristic of boiling obliterating any trace of the instanton.

.000	.002	.003	.002	.001	.000
.001	.006	.033	.025	.004	.001
.003	.032	.245	.245	.020	.002
.002	.021	.245	.206	.016	.002
.001	.004	.018	.014	.003	.001
.000	.001	.002	.002	.001	.000

TABLE 2
The same run as shown in Table 1 after several hundred sweeps at zero temperature. The lattice has settled down to an instanton.

successful, the topological charge should still be one. Table 2 shows the same run after several hundred sweeps at zero temperature. The lattice has settled down to an instanton, and it will go no further.

Runs with epsilon greater than .25 did not prevent tunneling. The boiled instanton, when refrozen, would settle down to the vacuum (all plaquette energies equal to zero). Since a plaquette has an energy between 0 and 1, restricting each plaquette to be below .25 energy is too constricting for most applications. There are, however, regimes of very high B which may still allow the use of the epsilon constraint without significantly hampering the lattice dynamics.

An alternative method of keeping down the energy density is to restrict the sum of the actions of the plaquettes surrounding any single link to be less than some value (again called epsilon). This condition will also suppress tunneling and is less restrictive than the first condition. The new epsilon should be about six times the old value. Our results indicate a new value of epsilon of about 1.5. A preliminary comparison of the results using this new epsilon condition seems quite encouraging.

If the new epsilon condition proves still to be too restrictive, its effect can be lessened by going to larger lattice sizes. It is unlikely that the increased time needed for larger lattices will negate the advantages gained by our method. Epsilons just under the critical value, while still allowing tunneling, did restrict it so that the system did not tunnel until nearly 1500 sweeps. Perhaps enforcing a relatively weak epsilon condition will be innocuous enough not to affect the behavior of the statistics of the lattice, but will slow the tunneling such that checks of the topological charge need be made less often. This will still greatly improve the prospects for the study of instantons on the lattice.

REFERENCES

(1) W. Marciano and H. Pagels, Physics Reports, 36c, No. 3.

(2) H. Goldstein, Classical Mechanics, Addison-Wesley, 1950.

(3) A.A. Belavin, A Polyakov, A. Schwarts, and Y. Tyupkin, Physics Letters, 59b, 85.

(4) C. 't Hooft, Physical Review Letters, 37, 8.

(5) M. Cretuz, L. Jacobs, and C. Rebbi, Physics Reports, 95, No. 4.

(6) P. Woit, Physical Review Letters, 51, 638.

(7) F. Fucito and S. Solomon, Nuclear Physics, B251, 505.

FACULTY SPONSOR OF THIS PAPER

Dr. Sorin Solomon
Department of Theoretical Physics
Caltech
Pasadena, CA 91125

A COMPREHENSIVE STUDY AND ANALYSIS OF A SIGMA PI SIGMA LAPEL PIN USING X-RAY FLUORESCENCE

R.A. Avedisian and B.K. Bellis
Physics Department
California State University, Fresno
Fresno, CA 93740

ABSTRACT

We determined the chemical composition of a Sigma Pi Sigma lapel pin using X-ray flourescence. From our results it can be stated that "old gold" is largely coppper with small amounts of nickle, zinc, and of course, gold.

In this experiment, the composition of a Sigma Pi Sigma lapel pin was determined using X-ray fluorescence analysis. Three different pins were analyzed, each providing essentially the same results. The analyses were done using the direct fluorescence method. The system used to find the content of the pins consisted of a modified Hewlett-Packard X-ray machine, an Ortec X-ray detector and a Tracor-Northern 1750 multichannel analyzer. The exposures were for 300 seconds with an operating potential of 30 kV and a tube current of 2.5 ma.

Figure 1 is a semi-log plot of counts vs X-ray energy. The semi-log plot enhances the peaks of the less abundant elements. The peaks are labeled in ascending order of energy. Peak one is from atmospheric argon. Peak two is from the titanium collimator in the X-ray path. Table 1 identifies the remaining peaks due to the elements in the pin.

Peak Number	Element
3	Iron
4	Nickel
5 & 7	Copper
6	Zinc
8 & 9	Gold

TABLE 1

Identification of peaks in Figure 1

Peaks 10 and 11 are from the detector summing of the copper-nickel and copper-copper peaks respectively.

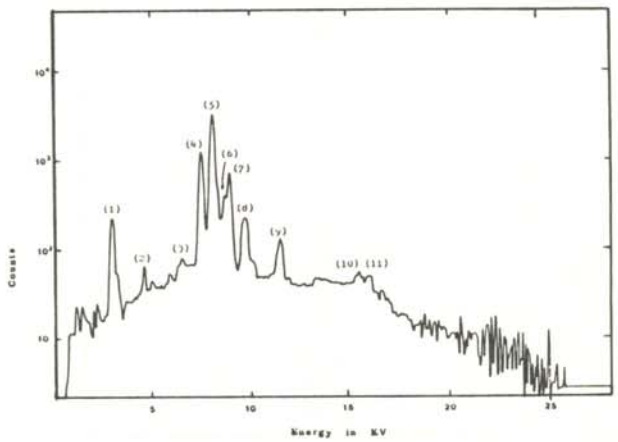

FIGURE 1
A semi-log plot of Counts vs Energy for the X-ray fluorescence spectrum of a Sigma Pi Sigma lapel pin. Table 1 identifies the peaks labled on the graph.

Element	Counts under peak
copper	115,000
nickel	31,000
gold	3,100
zinc	2,900
all others	<1,000

Table 2

Net counts under the peaks in Figure 1. The number of counts is directly related to the relative abundance.

The relative abundances of the elements can be estimated by the total number of counts under each peak. Table 2 shows the net counts under each of the peaks. This shows that the primary constituents of the pin are copper and nickel. There are also trace amounts of zinc, gold and iron present. Figure 2, a plot of counts vs. X-ray energy using a linear scale, clearly shows the relative abundance of each element in the lapel pin. Since the pin is made of "old gold", it can be stated that "old gold" is largely copper with very small amounts of gold present.

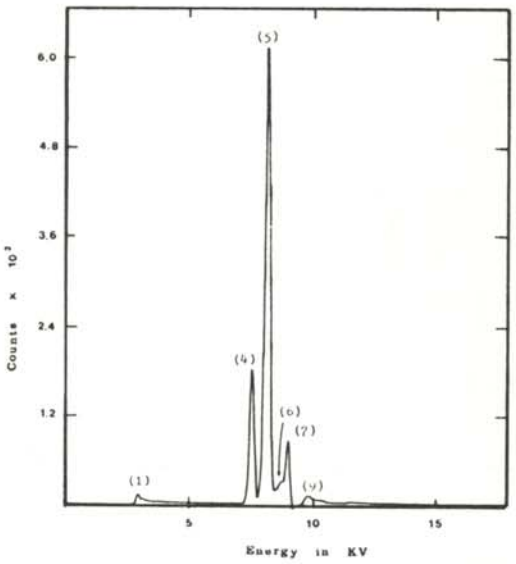

FIGURE 2
A linear plot of the data shown in Figure 1. This shows well the relative abundance of the elements in the Sigma Pi Sigma lapel pin. See Table 1 for identification of the peaks.